TRENDS IN SCIENCES 2026; 23(9): 13154
https://doi.org/10.48048/tis.2026.13154 RESEARCH ARTICLE

Effect of ZnO/gamma Chitosan Nanocomposites for Antifungal Activity on *Phytophthora palmivora*, a Disease-causing Fungus Using Para Rubber Trees

Wilaiwan Chaisorn[1], Nunticha Limchoowong[2], Phitchan Sricharoen[3,4], Prawit Nuengmatcha[5], Paweena Porrawatkul[5], Rungnapa Pimsen[5] and Arnannit Kuyyogsuy[5,*]

[1]*Department of Biology, Faculty of Science and Technology, Nakhon Si Thammarat Rajabhat University, Nakhon Si Thammarat 80280, Thailand*
[2]*Department of Chemistry, Faculty of Science, Srinakharinwirot University, Bangkok 10110, Thailand*
[3]*Division of Health, Cosmetic and Anti-Aging Technology, Faculty of Science and Technology, Rajamangala University of Technology Phra Nakhon, Bangkok 10800, Thailand*
[4]*Nuclear Technology Research and Development Center, Thailand Institute of Nuclear Technology (Public Organization), Nakhon Nayok 26120, Thailand*
[5]*Center of Excellence in Nanomaterials Chemistry, Department of Chemistry, Faculty of Science and Technology, Nakhon Si Thammarat Rajabhat University, Nakhon Si Thammarat 80280, Thailand*

([*]Corresponding author's e-mail: anannit_khu@nstru.ac.th)

Received: 25 December 2025, Revised: 2 February 2026, Accepted: 15 February 2026, Published: 5 April 2026

Abstract

In this study focused on the antifungal activity of Zinc oxide nanoparticles (ZnO NPs) and ZnO/gamma chitosan nanocomposites (ZnO/γ-Chi NCs) against *Phytophthora palmivora*, a disease-causing fungus that affects para rubber trees. The phase purity, crystallite size, morphology, chemical composition, and optical absorption properties of the synthesized materials were examined using various techniques. The X-ray diffraction (XRD) analysis revealed characteristic diffraction peaks corresponding to the crystal planes of the hexagonal wurtzite structure of ZnO NPs, which have the particle size of 31 nm. Moreover, they have confirmed the composite of both ZnO NPs and γ-chitosan. The FTIR spectroscopy was recorded the successful interaction between ZnO NPs (31 nm) and γ-chitosan (γ-Chi), which chitosan exposed to gamma radiation at sterilizing dosages of 40 kGy. The SEM and TEM images observed clusters of rod-shaped particulates for the ZnO/γ-chitosan NCs; according to the EDS profile, they confirmed the synthesis of ZnO/γ-chitosan NCs which found that nitrogen composition in the structure. UV-vis absorption spectra revealed a shift in the optical absorption toward lower wavelengths for the ZnO/γ-Chi NCs (355 nm) than for the ZnO NPs (365 nm). Upon assessing the antifungal activity, the results showed that ZnO/γ-Chi NCs were effective against *P. palmivora*, with an inhibition percentage of 90%. The SEM images showed that the damage to the fungal cell membrane caused by ZnO/γ-Chi NCs treatment significantly altered the outer shape of *P. palmivora*. These findings indicated that γ-chitosan and ZnO NPs may complement each other, exhibiting synergistic effects.

Keywords: ZnO/gamma chitosan nanocomposites, Zinc oxide nanoparticles, Characterization, *Phytophthora palmivora*, Antifungal activity, Para rubber tree, Disease

Introduction

The para rubber tree (*Hevea brasiliensis* Muell. Arg) is a crop of significant commercial value in Thailand. Natural rubber, a vital raw resource for polymers used in various items worldwide, can be produced by para rubber trees. Thailand continues to be the world's top producer and exporter of natural rubber as of 2025, accounting for about 36% of the total. It is anticipated that Thailand will produce about 4.93 million tons. Moreover, for comparison, the value of

rubber and rubber-related items exported in early 2024 was close to $19.2 billion USD [1]. These trees thrive in wet tropical lowlands (at elevation below 400 m) that are encircled by lush tropical rainforests [2]. In terms of income, Southeast Asian farmers are also interested in rubber plantations [3]. Pathogens can easily damage rubber tree seedlings during the nursery stage of growth. Specifically, fungal diseases, which thrive in humid, tropical environments, play a key role in slowing plantation growth, leading to economic loss. Leaf fall disease, attributed to fungus of the genus *Neopestalotiopsis* and fungal-like organisms in the genus *Phytophthora*, is among the most widespread fungal afflictions in para rubber trees [4,5]. *P. palmivora* is a destructive oomycete pathogen that affects rubber trees and seedlings, causing leaf fall and black stripe diseases, which can strongly affect plant growth during their development period [6-8]. Current disease management for para rubber trees using chemical fungicides can inhibit *P. palmivora*; however, while they are more effective, they also pose risks to beneficial soil microorganisms, the environment, and human health. Moreover, there is a growing concern about resistance development to disease [9]. The advancements in inorganic nanoparticle and chitosan research suggest the potential for the integration of enhanced antimicrobial agents, which might help reduce or even stop the application of fungicides detrimental to environmental and human health [10].

In recent years, researchers have developed antimicrobial agents made of natural or synthetic materials that are affordable and eco-friendly. Specifically, inorganic nanoparticles have generated much interest because of their potent and broad-spectrum antimicrobial properties [11]. The inorganic nanoparticles (NPs) silver, copper, CuO, TiO_2, $Mg(OH)_2$, and ZnO have strong antimicrobial activity. ZnO nanoparticles are of special importance because they can be produced quickly and affordably. Additionally, ZnO is a nontoxic and biocompatible substance that can serve as an effective photocatalyst and an antimicrobial agent because it can effectively oxidize organic contaminants and organisms [12]. ZnO exhibits potent antibacterial properties at neutral pH and biocidal effects on bacterial and fungal species at extremely low concentrations, indicating potential new uses in biomedicine, agriculture, and catalysis [13,14]. To enhance ZnO for antibacterial activity, recent research has concentrated on modifying its characteristics through noble metal loading, transition metal doping, and semiconductor coupling [15,16]. Chitosan is a deacetylated derivative of chitin, a copolymer that includes a collection of heteropolysaccharides made up of N-acetyl D-glucosamine and b-1,4-linked D-glucosamine residues. The deacetylation degree (DD) of chitin is generally between 40% and 98%. It is a naturally occurring polysaccharide and a major structural element of crustacean shells, insect exoskeletons and fungal cell walls [17,18]. Chitosan and its derivatives are employed as emulsifying, antimicrobial, antioxidant, stabilizing, and growth-promoting agents in a variety of chemical and related industries, including environmental protection, agriculture, biotechnology, pharma, food, cosmetics, and medicine, due to their biocompatible, biodegradable, and nontoxic polymer nature. As a result, chitosan has garnered significant attention as a functional biopolymer [19-21]. The DD of chitosan, its molecular weight (Mw), and its solution pH significantly affect its functional and physicochemical characteristics. Low-Mw chitosan is more soluble than high-Mw chitosan and has growth-stimulating, antioxidant, and antibacterial properties [22]. Chitosan is broken down by acidic and alkaline conditions. Despite their efficiency, these processes have drawbacks, including limited productivity and selectivity (acidic and alkaline), high processing costs (enzymatic), and the generation of toxic chemical wastes (acidic and alkaline) [23]. Radiation, which converts polysaccharides to oligomers without the use of potent chemical reagents, is a useful alternative strategy to overcome these restrictions [24]. In another study, gamma irradiation effectively broke down chitosan, cellulose, alginate, and starch by rupturing the glycosidic bond between the C1 and C4 sites of monomeric sugar residues, resulting in the production of matching oligomers [25]. Gamma chitosan (γ-Chi) is a superior biomaterial characterized by increased water solubility and bioactivity. The irradiation procedure aims to induce structural alterations in chitosan, leading to an augmented surface area and improved functional groups that promote stronger binding interactions with

particles. It acquires an enhanced capacity to suppress fungus, augment plant immunity, and the environmentally friendly derivative provides a potent, non-toxic option for sophisticated agricultural applications [26]. However, the effects of radiation on chitosan have not been fully described. Several techniques can be used to apply these oligomers to plants, such as foliar spraying, growth medium fortification, and root and shoot fortification. These applications can increase plant tolerance to biotic and abiotic stress and promote antibacterial activity [27]. Because chitosan can chelate with metals, it can interact with various metal oxides, including ZnO, TiO_2, Cu_2O, and CdS. Consequently, a nanocomposite of chitosan radiation and metal oxides can be produced for use [28,29]. Moreover, chitosan/ZnO nanoparticle composite coatings have higher antimicrobial activity than chitosan [30].

This study investigated the effects of ZnO NPs and ZnO/γ-Chi NCs and their properties. The major aims of this study were to (i) synthesize ZnO rod-shaped/γ-chitosan nanocomposites; (ii) characterize ZnO rod-shaped/γ-chitosan nanocomposites; and (iii) test antifungal activity in laboratory experiments using *P. palmivora*, a disease-causing fungus that affects para rubber trees. We specifically examined the impacts of ZnO nanoparticles (ZnO NPs) and ZnO/γ-chitosan nanocomposites (ZnO/γ-Chi NCs) with an emphasis on their structural and biological features in order to emphasize the novelty of the current study. This paper presents rod-shaped ZnO/γ-chitosan nanocomposites, a morphology and formulation that have not been thoroughly investigated for agricultural pathogen control, in contrast to earlier studies that mainly concentrate on spherical ZnO or traditional chitosan complexes. This comprehensive method offers fresh perspectives on the possible application of γ-chitosan composites based on zinc oxide nanoparticles as long-term antifungal agents for crop protection.

Materials and methods

Co-precipitate method for ZnO nanoparticles

To synthesize the ZnO nanoparticles, the zinc acetate dihydrate [$Zn(CH_3COO)_2 \cdot 2H_2O$] was dissolved in 40 mL of distilled water. The mixture was sonicated for 10 min until it became fully transparent. The pH was then adjusted with 1 M NaOH until it reached pH 10. The solution was continuously stirred for 30 min before being heated in an oil bath for 3 h at 50 °C until a white precipitate formed. The sediment was then filtered and washed several times with distilled water until the pH was neutral. After the sediment was obtained, it was dried for 8 h at 80 °C until completely dry. The dried sediment was ground in a mortar for use in the experiment.

Preparation of ZnO/γ-chitosan nanocomposites

We obtained γ-chitosan from the Thailand Institute of Nuclear Technology (Public Organization) Ongkharak, Nakhon Nayok, Thailand. Chitosan subjected to gamma radiation at sterilization dosages of 40 kGy. The γ-chitosan had a molecular weight of 190 kDA and a 95% degree of deacetylation (DD). Briefly, the synthesized ZnO nanoparticles (1 g) were first dissolved in 100 mL of 1% (v/v) acetic acid to prepare ZnO/γ-Chi NCs. This solution was supplemented with 750 mg of γ-chitosan. After the mixture was sonicated for 20 min, 1 M NaOH (Sigma Aldrich, USA) was added dropwise until the pH reached 10. The solution was heated for 3 h in a water bath at 65 °C. Finally, the precipitate was filtered, washed several times with distilled water, and dried for 6 h in an oven at 50 °C.

Characterization of ZnO NPs and ZnO/γ-chitosan nanocomposites

UV-vis absorption spectra were recorded in the wavelength range of 300 - 700 nm using a spectrophotometer (Mecasys, Republic of Korea). The FTIR analysis was performed using the (Perkin-Elmer; Bruker Tensor 27, Germany) in the 4,000 to 500 cm^{-1} region to confirm the presence of functional groups of ZnO/γ-Chi NCs. The XRD analysis were conducted using a Philips PW-1710 diffractometer with CuKα radiation (λ= 1.5406) (Philips X'PERT MPD, Netherlands). SEM analysis was performed at a 10 kV accelerating voltage using (Hitachi S-4800, Japan). TEM was performed at a 300 kV operating voltage to using the Technai (G2 F30 S-Twin, FEI, USA). EDS attached with SEM was performed to determine the elemental composition (JEOL JSM-700F-EDS, USA).

Antifungal assays

P. palmivora was obtained from Department of Biology, Faculty of Science and Technology, Nakhon Si Thammarat Rajabhat University, Nakhon Si Thammarat, Thailand, in cooperation with the Songkhla Rubber Research Center, Songkhla, Thailand. The synthesized ZnO NPs and ZnO/γ-Chi NCs were mixed with potato dextrose agar (PDA) and poured into Petri dishes to obtain final concentrations of 0.05, 0.10, and 0.15 mg/mL.

The effects of 3 concentrations (0.05, 0.10 and 0.15 mg/mL) of the synthesized ZnO NPs and ZnO/γ-Chi NCs on *P. palmivora* growth were determined. Discs (4 mm) of fungal mycelia from the growing edges of a 5-day-old culture of *P. palmivora* were placed on PDA plates and incubated for 10 days at room temperature. The growth diameters (mm) were measured and are presented as the percentage of inhibition [31]. Each treatment was replicated using 3 plates, and the experiment was performed 3 times.

$$\%\ inhibition = 100 - \left[\left(\frac{R^2}{r^2}\right) \times 100\right]$$

where, R is radial to the fungal colonies for the control, and r is radial to the fungal colonies for the treatment.

The morphological changes in *P. palmivora* after treatment with ZnO NPs and ZnO/γ-Chi NCs were investigated via SEM.

Statistical analyses

All data pertaining to the antifungal activity test was presented as means ± SD for triplicates. Statistical investigation utilized an unpaired 2-tailed t-test to determine the significant difference between the treatment of ZnO NPs and ZnO/γ-Chi NCs on the growth of *P. palmivora*. Significant differences were established at $p < 0.05$.

Results and discussion

Characterization of ZnO/γ-Chi NCs

The UV-vis absorption spectra of the ZnO NPs and ZnO/γ-Chi NCs (**Figure 1**) exhibited similar absorption profiles with minor differences in their absorption maxima. Owing to the lack of conjugated double bonds in the chitosan molecule [32]. The ZnO NPs have intrinsic band-gap absorption as a result of electrons moving from the valence band to the conduction band (O_{2p} to Zn_{3d}) showed a maximum absorption at 365 nm, which was attributed to the intrinsic band-gap absorption of the ZnO NPs [33]. However, because of the interaction with γ-chitosan, the absorption has shifted to 355 nm for the ZnO/γ-Chi NCs.

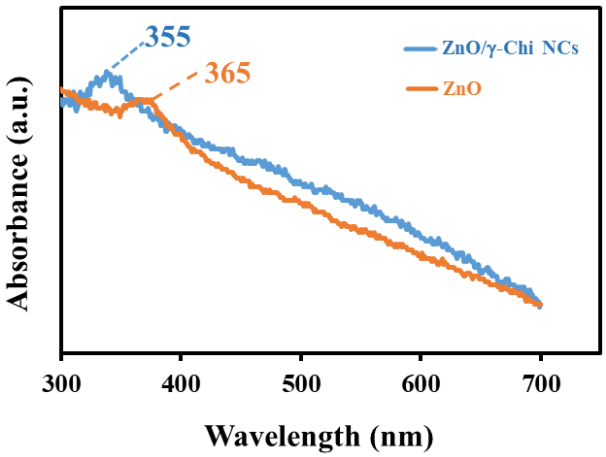

Figure 1 UV-vis absorption spectrum of ZnO NPs and ZnO/γ-Chi NCs.

The FTIR spectra of γ-chitosan (γ-Chi), ZnO NPs and ZnO/γ-Chi NCs are presented in **Figure 2**. The γ-chitosan spectrum shows a broad band at 3,495 cm^{-1} attributed to overlapping O–H and N–H stretching vibrations, along with a peak at 2,876 cm^{-1} corresponding to C–H stretching. The absorption band at 1,555 cm^{-1} is assigned to the amide II vibration arising from N–H bending and C–H stretching, while the peak

at 1,408 cm^{-1} is associated with CH_3 bending or C–H stretching. The band observed at 1,021 cm^{-1} corresponds to C–O stretching vibrations characteristic of the polysaccharide backbone [34]. The FTIR spectrum of ZnO NPs exhibits a characteristic Zn–O stretching vibration at 367 cm^{-1}. In the ZnO/γ-Chi NCs, noticeable peak shifts and intensity changes were observed, indicating interactions between ZnO NPs and γ-chitosan. The shift of the O–H/ N–H stretching band to 3,440 cm^{-1} and the appearance of a new band at 355 cm^{-1}, attributed to O–Zn–O stretching, confirm coordination between ZnO and the hydroxyl and amine groups of chitosan [35]. These results verify the successful incorporation of ZnO NPs into the γ-chitosan matrix.

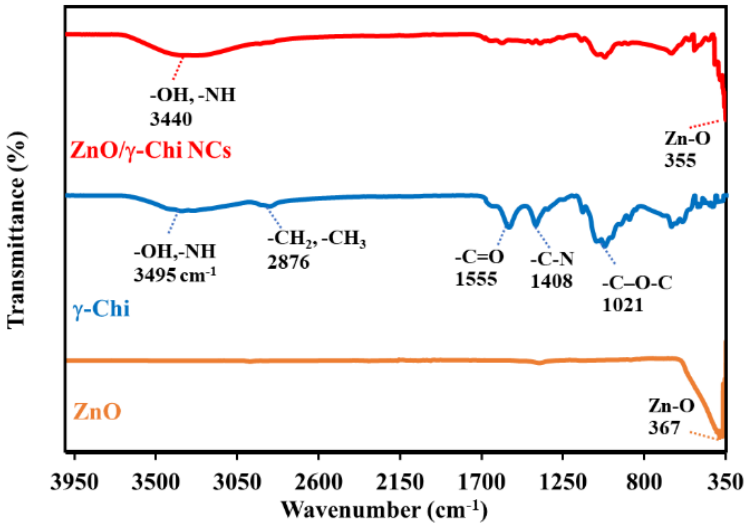

Figure 2 FTIR band spectrum of synthesized ZnO NPs, γ-chitosan (γ–Chi) and ZnO/γ-Chi NCs**.**

The XRD patterns of γ-chitosan, ZnO NPs, and ZnO/γ-Chi NCs are shown in **Figure 3**. γ-chitosan exhibits 2 characteristic diffraction peaks at 2θ = 10° and 20°, which correspond to the semi-crystalline nature and fingerprint structure of chitosan. The XRD pattern of ZnO NPs displays distinct diffraction peaks at 2θ values of 31.74°, 34.40°, 36.23°, 47.51°, 56.55°, 62.82°, 66.32°, 67.89°, 69.03° and 76.89°, which can be indexed to the (1 0 0), (0 0 2), (1 0 1), (1 0 2), (1 1 0), (1 0 3), (1 1 2), (2 0 1), and (2 0 2) planes of the hexagonal wurtzite structure of ZnO (JCPDS data card no. 36–1451) [36–38]. The average crystallite size of ZnO NPs was calculated using the Debye Scherrer equation [39],

$$D = \frac{K\lambda}{\beta\cos\theta}$$

where, D is the average particle size (nm), λ is the wavelength of X-ray used (1.54060 Å), K is the constant (0.9), β is the full line width at the half-maximum elevation of the main intensity peak, and θ is the Bragg's angle.

The size of the particles was estimated to be approximately 31 nm for nanoparticles synthesized via the co-precipitation method. In the ZnO/γ-Chi NCs, diffraction peaks corresponding to both ZnO NPs and γ-chitosan were observed, confirming the formation of the nanocomposite. The retention of ZnO diffraction peaks indicates that crystalline structure of ZnO remained intact after incorporation into the γ-chitosan matrix. Minor peak broadening and intensity variations suggest physical interaction or surface bonding between ZnO NPs and chitosan chains.

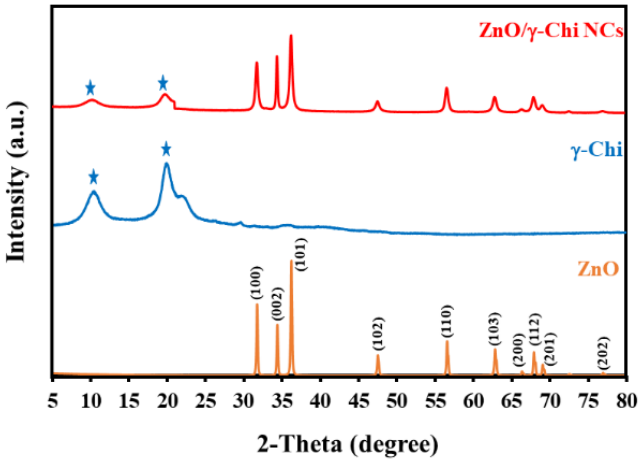

Figure 3 XRD pattern of γ-chitosan (γ–Chi), ZnO NPs, and ZnO/γ-Chi NCs.

The SEM and EDS spectra of the ZnO NPs and ZnO/γ-Chi NCs are shown in **Figure 4**. The SEM images revealed that the ZnO NPs were rod-shaped particles with well-defined borders (**Figure 4(A)**). The EDS profile of the ZnO NPs (**Figure 4(C)**) was dominated by Zn and oxygen (O), indicating that the produced product contained no additional elemental contaminants. The carbon (C) peak in the EDS profile occurred due to the carbon tape that was used to load the samples. The SEM image of ZnO/γ-Chi NCs (**Figure 4(B)**) revealed a cluster-like morphology generated by the aggregation of different-sized particles. The EDS profile (**Figure 4(D)**) further confirmed the synthesis of ZnO/γ-Chi NCs, with γ-chitosan contributing along with ZnO. Nitrogen (N) was present probably due to the amine (-NH_2) group of γ-chitosan, along with Zn and O. Due to the interaction of ZnO with γ-chitosan, a morphological study revealed that adding γ-chitosan induced a slight alteration in morphology [40]. This assumption is also supported by TEM analyses. Indeed, the observed fringes in the TEM image shown in **Figure 5** correspond to a d-spacing of 0.02605 nm, which is equal to the theoretical ZnO (0 0 2) distances [41].

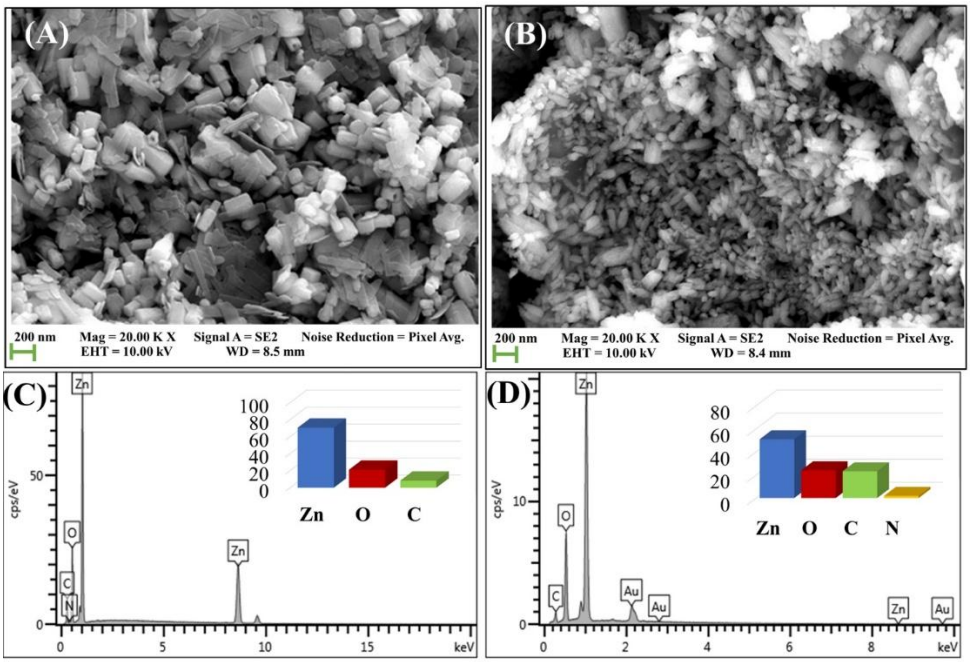

Figure 4 SEM image of (A) ZnO NPs, (B) ZnO/γ-Chi NCs and EDS data of (C) ZnO NPs (D) ZnO/γ-Chi NCs.

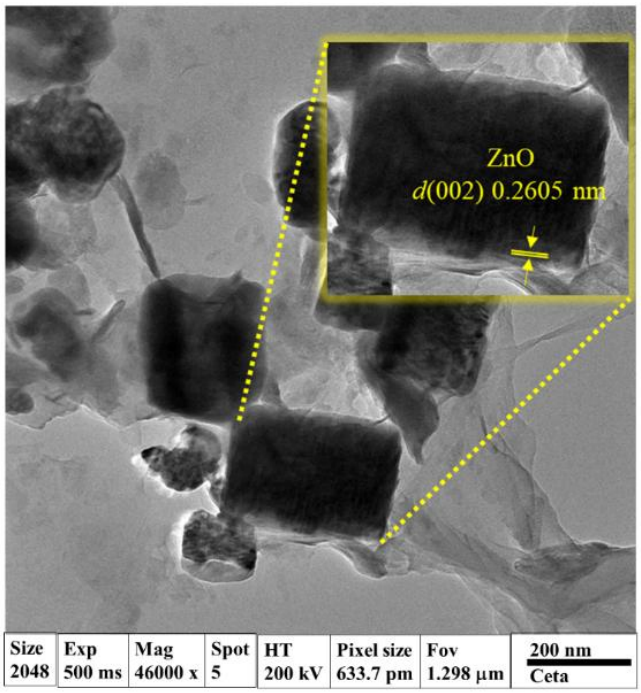

Figure 5 TEM image of ZnO/γ-Chi NCs.

Antifungal activity of the synthesized ZnO/γ-Chi NCs

The growth of *P. palmivora* on media containing different concentrations of ZnO NPs and ZnO/γ-Chi NCs is shown in **Figure 6**. The mycelial growth of *P. palmivora* was suppressed by media containing more ZnO/γ-Chi NCs than by media containing more ZnO NPs. These results indicated that the degree of inhibition depended on the concentration of γ-chitosan in the fungal growth medium. When comparing the results, 2 commercial fungicides were assessed for their efficacy against the *P. palmivora* by the poisoned food technique. Among all the fungicides tested at 0.2% concentration, Dimethomorph 9% mixed with Mancozeb 60% WP and Fosetyl-AL 80 WP showed 19.29% and 88.88% inhibition, respectively. ZnO/γ-Chi NCs can hence inhibit more effectively [42]. For **Figure 7**, The greatest mycelial growth inhibition was found in the medium containing 0.15 mg/mL ZnO/γ-Chi NCs, with a maximum inhibition of about 90%, whereas in the medium containing 0.15 mg/mL ZnO NPs, 52% inhibition occurred after 10 days. The results of this study showed a high level of efficacy compared to previous research. The ZnO NPs exhibit antifungal activity against *P. palmivora*, the causal agent of durian stem and root rot. At a concentration of 2,000 µg/mL, the ZnO NPs inhibited the mycelial growth of isolates Phy001 and Phy002 by 56.6% and 53.6%, respectively, and reduced disease severity on durian leaves by 50.5% and 43.7%. These results confirm the ability of ZnO NPs to interfere with vegetative growth and pathogenicity of *P. palmivora* [43]. However, inhibition was incomplete, suggesting that ZnO NPs may require higher concentrations to provide effective control under natural conditions. When applied at 2,000 mg/mL, ZnO NPs suppressed mycelial growth of all fungal isolates tested, with inhibition ranging from 57.76% - 69.84%. This indicates a clear dose-dependent antifungal effect, consistent with previous findings that higher ZnO NPs concentrations enhance antifungal efficacy via increased release of Zn^{2+} ions and generation of reactive oxygen species (ROS), which damage cell membranes and organelles [44-46]. Previous studies on *Fusarium oxysporum*, *Alternaria alternata*, and *Colletotrichum* spp. have reported strong inhibition of mycelial growth and spore germination at comparable or lower concentrations of ZnO NPs [47,48]. Compared to these pathogens, *P. palmivora* appears relatively more tolerant, possibly due to its robust cell wall structure and effective ROS detoxification mechanisms.

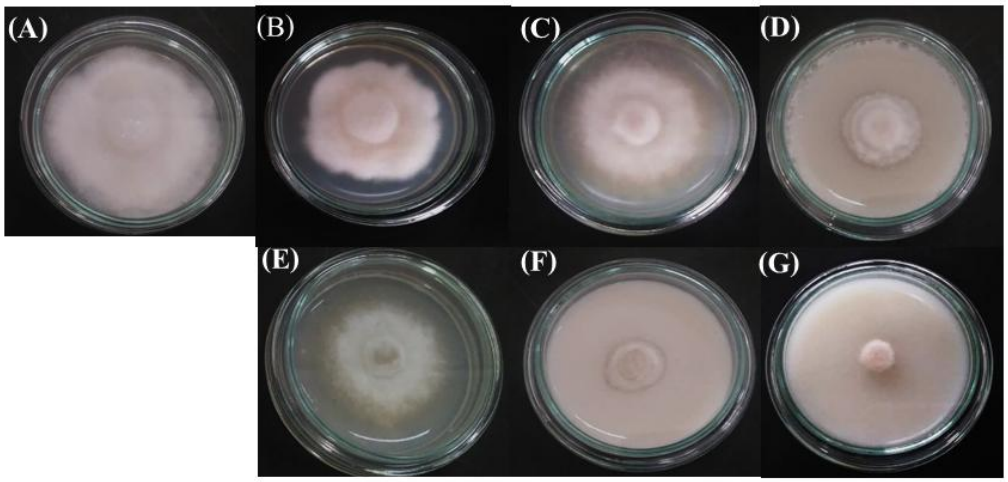

Figure 6 Antifungal activity; effect of control (A), 3 concentrations (0.05, 0.10 and 0.15 mg/mL) of the ZnO NPs (B-D), and the synthesized ZnO/γ-Chi NCs (E-G) on the growth of *P. palmivora* after 10 days.

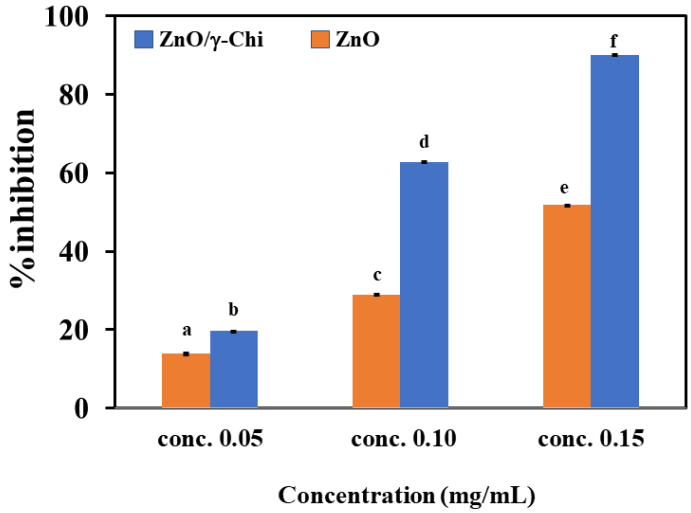

Figure 7 Percentage inhibitory effects of three concentrations (0.05, 0.10 and 0.15 mg/mL) of the synthesized ZnO NPs and ZnO/γ-Chi NCs on the growth of *P. palmivora* after 10 days. The different letters used indicate significant differences ($p \leq 0.05$) for the treatment of ZnO NPs and ZnO/γ-Chi NCs. Data represent the mean (± standard deviation, SD).

Morphological changes in *P. palmivora* treated with ZnO/γ-Chi NCs

The morphological changes in *P. palmivora* mycelia after treatment with ZnO NPs and ZnO/γ-Chi NCs were also evaluated via SEM analysis and compared to those of the control. The morphological changes in *P. palmivora* mycelia following treatment with ZnO NPs and ZnO/γ-Chi NCs are shown in **Figure 8**. Changes in morphology between the treated and untreated (control) fungi were found in the SEM images. The control *P. palmivora* (**Figure 8(A)**) exhibited a characteristic filament-shaped cell state with a smooth membrane surface. After treatment with ZnO NPs and ZnO/γ-Chi NCs at a concentration of 0.15 mg/mL (**Figures 8(B)** and **8(C)**), the cell membrane started to bulge and lose its smoothness, impairing the integrity of the cell membrane. When the cell membrane ruptured, the fungal shape changed considerably from filamentous to deformed.

The antimicrobial activity of ZnO NPs can be explained by several processes, including (i) the release of Zn^{2+} cations from the surface of the particles, (ii) direct interaction with microbial cells, (iii) penetration through the cell membrane, and (iv) the production of reactive oxygen species (ROS), including hydrogen peroxide (H_2O_2), superoxide anions ($\bullet O_2^-$), and

hydroxyl radicals (•OH), which harm the intracellular components and the cell membrane [49,50]. Although each of these elements plays a key role in the antimicrobial action of ZnO NPs, the precise mechanism needs to be elucidated. Owing to the large particle size and minimal Zn^{2+} ion dissolution under such conditions, the antifungal activity of ZnO NPs resulting from particle penetration and the release of Zn^{2+} ions may be ruled out. The direct interaction of the ZnO NPs or ZnO/γ-Chi NCs resulted in surface bulging, damage to the cell membrane, and damage to the cell structure, as shown by the SEM image (**Figure 8**). ZnO NPs produce active oxygen species ($•O_2$) in gloomy environments and form ROS under light illumination [51]. Therefore, the antifungal activity observed may be due to any one of the aforementioned mechanisms acting alone or in combination. Additionally, because of an increase in coulombic attraction, the combination of ZnO with chitosan improved antifungal effectiveness. Owing to the presence of the NH_2 group, chitosan is a cationic polymer and can bind to metal ions strongly with the help of positively charged NH_2 groups [52,53]. Consequently, the positive charge is strengthened by the formation of ZnO/γ-Chi NCs, which increases the electrostatic contact with the negatively charged cell membrane. The significantly damaged cell structure of the fungi compared to that of the ZnO particle-treated cells revealed the extent of damage caused by an increase in the electrostatic interaction of ZnO/γ-Chi NCs. The cytotoxicity of ZnO nanoparticles and ZnO chitosan nanocomposites was assessed in HEp2 cells, revealing that ZnO chitosan nanocomposites exhibited lower cytotoxicity than ZnO, which had dose-dependent cytotoxicity. The material had no significant reduction in cell viability at low concentrations (< 6.25 µg/mL) but marked toxicity at higher concentrations (≥ 12.5 µg/mL) [54]. The foliar application of ZnO NPs in rice plants demonstrated that the xylem and phloem are the organs responsible for the translocation and transformation of ZnO nanoparticles after uptake by rice leaves, thereby confirming the efficacy and safety of this application method [55].

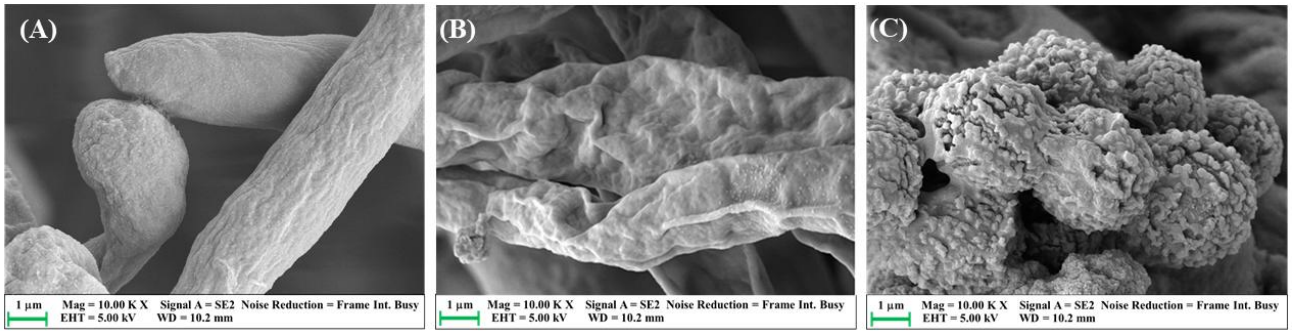

Figure 8 SEM image of the antifungal activity of H_2O (control) (A), ZnO NPs (B), and ZnO/γ-Chi NCs (C) against *P. palmivora.*

Mechanism of ZnO/γ-Chi NCs against *P. palmivora*

The schematic illustrates (**Figure 9**) the proposed mechanism by which the ZnO/γ-chitosan NCs inhibits the growth of *P. palmivora*, a fungal pathogen affecting plants. Firstly, γ-chitosan a derivative of chitosan, acts as a natural biopolymer containing abundant amino ($-NH_2$) and hydroxy (−OH) groups that can strongly combine with ZnO NPs through hydrogen bonding and electrostatic interactions. This functionalization progresses the dispersion, surface stability, and biocompatibility of ZnO particles. Upon light irradiation, the ZnO semiconductor generated electron hole pair. The photoexcited electron in the conduction band react with molecular oxygen (O_2) to form superoxide radicals ($•O_2^-$), while holes in the valence band react with water molecules (H_2O) or hydroxide ions (OH^-) to produce hydroxyl radicals (•OH) [56,57]. These reactive oxygen species (ROS) collectively contribute to strong oxidative stress. The ROS generated by ZnO/γ-chitosan attack the fungal cell membrane, protein, and nucleic acids, leading to severe cellular damage and inhibition of *P. palmivora* growth. The synergistic effect of ZnO photocatalytic ROS generation

and the natural antimicrobial property of γ-chitosan improve the antifungal efficiency of the composite [58,59]. The formation of ROS in ZnO occurred with light illumination; however, ZnO nanoparticles (NPs) can also generate active oxygen species ($\bullet O_2^-$) in the absence of light, as demonstrated by electron spin resonance spectroscopy [60]. The nanoparticle-induced ROS have been shown to markedly diminish sporangial germination, impede zoospore motility, decrease mycelial growth, and obstruct the creation of infection structures, hence restricting host colonization. Moreover, reactive oxygen species (ROS) impair mitochondrial respiration, leading to energy depletion and ultimately cell death. The ZnO/γ-chitosan NCs provide a sustainable and eco-friendly approach to control plant pathogenic fungi [61].

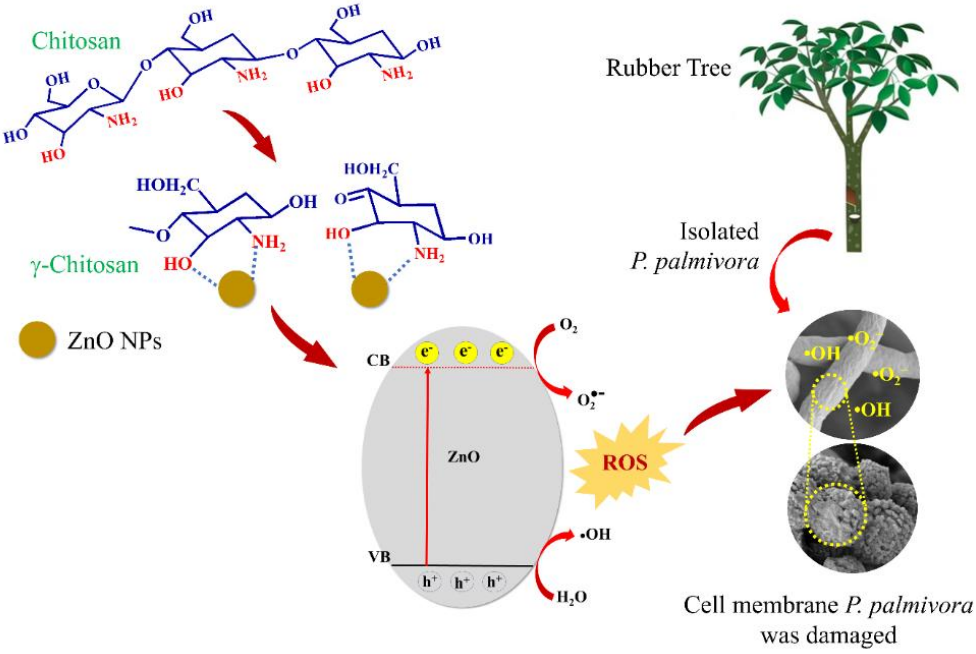

Figure 9 Schematic illustration of antifungal activity of ZnO/γ-chitosan NCs against *P. palmivora.*

Conclusions

In this study, ZnO rods-shaped were created using a wet chemical method in which zinc acetate dihydrate was used as a precipitating agent and then combined with γ-chitosan to form ZnO/γ-Chi NCs. ZnO rod-shaped and ZnO/γ-Chi NCs were investigated for their antifungal efficacy against *P. palmivora* (a model fungus) by assessing the percentage of inhibition and the degree of damage to the cell structure, as demonstrated by SEM images. The findings of this study showed that ZnO/γ-Chi NCs have greater antifungal effects on the tested fungus than ZnO NPs. According to our research, ZnO/γ-Chi NCs have the potential to replace current fungicides and be used as an efficient antifungal agent. In the future, foliar sprays of ZnO/γ-Chi NCs on para rubber tree leaves inhibited *P. palmivora*. Nevertheless, comprehensive long-term environmental and ecotoxicological studies are essential prior to large-scale agricultural application.

Acknowledgements

The authors would like to thank the Thailand Institute of Nuclear Technology (Public Organization) Ongkharak, Nakhon Nayok, Thailand, for the financial support. We are grateful for offering the equipment support required form the Center of Excellence in Nanomaterials Chemistry, Department of Chemistry, Faculty of Science and Technology, Nakhon Si Thammarat Rajabhat University, Thailand.

Declaration of generative AI in scientific writing

The authors acknowledge the use of generative AI tools (e.g., QuillBot and ChatGPT by OpenAI) in the

preparation of this manuscript, specifically for language editing and grammar correction. No content generation or data interpretation was performed by AI. The authors take full responsibility for the content and conclusions of this work.

CRediT author statement

Wilaiwan Chaisorn: Conceptualization, Methodology, Supervision, Validation and Writing-Original Draft. **Nunticha Limchoowong**: Data curation, Formal analysis and Validation. **Phitchan Sricharoen**: Data curation, Formal analysis and Validation. **Prawit Nuengmatcha**: Data curation, Formal analysis, Investigation and Validation. **Paweena Porrawatkul**: Data curation, Formal analysis, Investigation, Visualization and Validation. **Rungnapa Pimsen**: Data curation, Formal analysis, Investigation and Validation. **Arnannit Kuyyogsuy**: Conceptualization, Methodology, Software, Resources, Data Curation, Supervision, Project administration, Funding acquisition and Writing - Review & Editing.

References

[1] Association of Natural Rubber Producing Countries. Monthly NR statistical report, Available at: https://www.anrpc.org/news/anrpc-releases-monthly-nr-statistical-report%2C-september-2025, accessed September 2025.

[2] J Fox and JC Castella. Expansion of rubber (*Hevea brasiliensis*) in mainland Southeast Asia: What are the prospects for smallholders? *The Journal of Peasant Studies* 2013; **40(1)**, 155-170.

[3] Z Li and JM Fox. Mapping rubber tree growth in mainland Southeast Asia using time-series MODIS 250 m NDVI and statistical data. *Applied Geography* 2012; **32(2)**, 420-432.

[4] C Pornsuriya, T Chairin, N Thaochan and A Sunpapao. Identification and characterization of *Neopestalotiopsis* fungi associated with a novel leaf fall disease of rubber trees (*Hevea brasiliensis*) in Thailand. *Journal of Phytopathology* 2020; **168(7-8)**, 416-427.

[5] B Laohasakul, P Boonyapipat and P Plodpai. First report of *Phytophthora citrophthora* causing leaf fall of para rubber tree (*Hevea brasiliensis*) in Thailand. *Plant Disease* 2017; **101(6)**, 1057.

[6] N Churngchow and M Rattarasarn. Biosynthesis of scopoletin in *Hevea brasiliensis* leaves inoculated with *Phytophthora palmivora*. *Journal of Plant Physiology* 2001; **158(7)**, 875-882.

[7] U Krishnan, M Kaur, K Singh, M Kumar and A Kumar. A synoptic review of MoS2: Synthesis to applications. Superlattice. *Superlattices and Microstructures* 2019; **128**, 274-297.

[8] Y Saijo and EP Loo. Plant immunity in signal integration between biotic and abiotic stress responses. *New Phytologist* 2020; **225(1)**, 87-104.

[9] P Kongtragoul. *In vitro* fungicidal effect of chitosan with different molecular weights on fungicide-resistant *Phytophthora* fruit rot on durian from the export market. *Acta Horticulturae* 2018; **1210**, 65-72.

[10] V Tsikourkitoudi, B Henriques-Normark and GA Sotiriou. Inorganic nanoparticle engineering against bacterial infections. *Current Opinion in Chemical Engineering* 2022; **38**, 100872.

[11] SB Mayegowda, G Sarma, MN Gadilingappa, S Alghamdi, A Aslam, B Refaat, M Almehmadi, M Allahyani, AA Alsaiari, A Aljuaid and IS Al-Moraya. Green-synthesized nanoparticles and their therapeutic applications: A review. *Green Processing and Synthesis* 2023; **12(1)**, 20230001.

[12] AW Alshameri and M Owais. Antibacterial and cytotoxic potency of the plant-mediated synthesis of metallic nanoparticles Ag NPs and ZnO NPs: A review. *OpenNano* 2022; **8**, 100077.

[13] MNVR Kumar. A review of chitin and chitosan applications. *Reactive and Functional Polymers* 2000; **46(1)**, 1-27.

[14] F Shahidi, JKV Arachchi and YJ Jeon. Food applications of chitin and chitosans. *Trends in Food Science & Technology* 1999; **10**, 37-51.

[15] T Jan, J Iqbal, M Ismail and A Mahmood. Synthesis of highly efficient antibacterial agent Ag doped ZnO nanorods: Structural, raman and optical properties. *Journal of Applied Physics* 2014; **115(15)**, 154308.

[16] K Vijayalakshmi and D Sivaraj. Enhanced antibacterial activity of Cr doped ZnO nanorods synthesized using microwave processing. *RSC Advances* 2015; **5(84)**, 68461-68469.

[17] H Sashiwa and SI Aiba. Chemically modified chitin and chitosan as biomaterials. *Progress in Polymer Science* 2004; **29(9)**, 887-908.

[18] AB Muley, SA Chaudhari, KH Mulchandani and RS Singhal. Extraction and characterization of chitosan from prawn shell waste and its conjugation with cutinase for enhanced thermo-stability. *International Journal of Biological Macromolecules* 2018; **111**, 1047-1058.

[19] AB Muley, AS Thorat, SG Dalvi, MI Talib and VR Parate. Comparative studies and correlation between physicochemical and functional properties of chitosan from marine sources. *Trends in Biosciences* 2015; **8(22)**, 6267-6274.

[20] FCK Ocloo1, A Adu-Gyamfi, EA Quarcoo, Y Serfor-Armah, DK Asare and C Owulah. Effect of gamma irradiation on antibacterial properties of sea crab shell chitosan. *European Journal of Food Research & Review* 2012; **2(3)**, 69-78.

[21] I Perelshtein, E Ruderman, N Perkas, T Tzanov, J Beddow, E Joyce, TJ Mason, M Blanes, K Mollá, A Patlolla, AI Frenkel and A Gedanken. Chitosan and chitosan-ZnO-based complex nanoparticles: Formation, characterization, and antibacterial activity. *Journal of Materials Chemistry B* 2013; **1**, 1968-1976.

[22] A Charlesby. Crosslinking and degradation of polymers. *Radiation Physics and Chemistry* 1981; **18(1-2**), 59-66.

[23] LQ Luan and NHP Uyen. Radiation degradation of (1→3)-β-d-glucan from yeast with a potential application as a plant growth promoter. *International Journal of Biological Macromolecules* 2014; **69**, 165-170.

[24] I Zainol, HM Akil and A Mastor. Effect of γ-irradiation on the physical and mechanical properties of chitosan powder. *Materials Science and Engineering: C* 2009; **29(1)**, 292-297.

[25] M Cho, BY Kim and JH Rhim. Degradation of alginate solution and powder by gamma irradiation. *Food Engineering Progress* 2003; **7**, 141–145.

[26] S Mirajkar, P Rathod, B Pawar, S Penna and S Dalvi. γ irradiated chitosan mediates enhanced synthesis and antimicrobial properties of chitosan-silver (Ag) nanocomposites. *American Chemical Society* 2021; **6**, 34812-34822.

[27] TA Dar, M Uddin, MM Khan, A Ali, SA Mir and L Varshney. Effect of Co-60 gamma irradiated chitosan and phosphorus fertilizer on growth, yield and trigonelline content of *Trigonella foenum-graecum* L. *Journal of Radiation Research and Applied Sciences* 2015; **8(3)**, 446-458.

[28] KT Karthikeyan, A Nithya and K Jothivenkatachalam. Photocatalytic and antimicrobial activities of chitosan-TiO2 nanocomposite. *International Journal of Biological Macromolecules* 2017; **104**, 1762-1773.

[29] S Kumar, F Ye, S Dobretsov and J Dutta. Chitosan nanocomposite coatings for food, paints, and water treatment applications. *Applied Sciences* 2019; **9(12)**, 2409.

[30] L Al-Naamani, S Dobretsov, J Dutta and JG Burgess. Chitosan-zinc oxide nanocomposite coatings for the prevention of marine biofouling. *Chemosphere* 2017; **168**, 408-417.

[31] A Gamliel, J Katan and E Cohen. Toxicity of chloronitrobenzenes to *Fusarium oxysporum* and *Rhizoctonia solani* as related to their structure. *Phytoparasitica* 1989; **17**, 101-106.

[32] LH Li, JC Deng, HR Deng, ZL Liu and XL Li. Preparation, characterization and antimicrobial activities of chitosan/Ag/ZnO blend films. *Chemical Engineering Journal* 2010; **160(1)**, 378-382.

[33] M Shoeb, BR Singh, JA Khan, W Khan, BN Singh, HB Singh and AH Naqvi. ROS-dependent anticandidal activity of zinc oxide nanoparticles synthesized by using egg albumen as a biotemplate. *Advances in Natural Sciences: Nanoscience and Nanotechnology* 2013; **4**, 035015.

[34] A H Bashal, SM Riyadh, W Alharbi, KH Alharbi, TA Farghaly and KD Khalil. Bio-based (Chitosan-ZnO) nanocomposite: Synthesis, characterization, and its use as recyclable, ecofriendly biocatalyst for synthesis of thiazoles tethered azo groups. *Polymers* 2022; **14(3)**, 386.

[35] ER El-Sayed, HK Abdelhakim and Z Zakaria. Extracellular biosynthesis of cobalt ferrite nanoparticles by *Monascus purpureus* and their antioxidant, anticancer and antimicrobial

activities: Yield enhancement by gamma irradiation. *Materials Science and Engineering: C* 2020; **107**, 110318.

[36] I Perelshtein, Y Ruderman, N Perkas, K Traeger, T Tzanov, J Beddow, E Joyce, TJ Mason, M Blanes, K Molla and A Gedanken. Enzymatic pre-treatment as a means of enhancing the antibacterial activity and stability of ZnO nanoparticles sonochemically coated on cotton fabrics. *Journal of Materials of Chemistry* 2012; **22**, 10736-10742.

[37] SY Han, BK Paul and CH Chang. Nanostructured ZnO as biomimetic anti-reflective coatings on textured silicon using a continuous solution process. *Journal of Materials of Chemistry* 2012; **22**, 22906-22912.

[38] Y Qin, S Li, Y Li, F Pan, L Han, ZM Chen, XZ Yin, LX Wang and H Wang. Mechanically robust polybenzoxazine/reduced graphene oxide wrapped-cellulose sponge towards highly efficient oil/water separation, and solar-driven for cleaning up crude oil. *Composites Science and Technology* 2020; **197**, 108254.

[39] X Liu, J Tian, Y Li, N Sun, S Mi, Y Xie and Z Chen. Enhanced dyes adsorption from wastewater via Fe3O4 nanoparticles functionalized activated carbon. *Journal of Hazardous Materials* 2019; **373**, 397-407.

[40] SHS Dananjaya, RS Kumar, M Yang, C Nikapitiya, J Lee and M De Zoysa. Synthesis, characterization of ZnO-chitosan nanocomposites and evaluation of its antifungal activity against pathogenic *Candida albicans*. *International Journal of Biological Macromolecules* 2018; **108**, 1281-1288.

[41] P Porrawatkul, R Pimsen, A Kuyyogsuy, N Teppaya, A Noypha, S Chanthai and P Nuengmatcha. Microwave-assisted synthesis of Ag/ZnO nanoparticles using *Averrhoa carambola* fruit extract as the reducing agent and their application in cotton fabrics with antibacterial and UV protection properties. *RSC Advances* 2022; **12(24)**, 15008-150019.

[42] L Sindhu, K Gopal, K Arunodhayam, C Ruth and B Srinivasulu. Evaluation of fungicides against *Phytophthora palmivora in vitro*. *The Pharma Innovation Journal* 2022; **11(8)**, 776-779.

[43] K Jariyachawalid, P Laowanapiban, V Meevootisom and S Wiyakrutta. Effective enhancement of *Pseudomonas stutzeri* D-phenylglycine aminotransferase functional expression in *Pichia pastoris* by co-expressing *Escherichia coli* GroEL-GroES. *Microbial Cell Factories* 2012; **11**, 47.

[44] S Gurunathan, M Qasim, C Park, H Yoo, JH Kim and K Hong. Cytotoxic potential and molecular pathway analysis of silver nanoparticles in human colon cancer cells HCT116. *International Journal of Molecular Science* 2018; **19(8)**, 2269.

[45] A Popova, DY Advakhova, AN Shevevko, KA Kuptsov, P Slukin, SG Ignatov, A Ilniskava, RV Timoshenko, AS Erofeev, AA Kuchmizhak, B Subramanian and DV shtansky. Synergistic bactericidal effect of Zn^{2+} ions and reactive oxygen species generated in response to either UV or X-ray irradiation of Zn-doped plasma electrolytic oxidation TiO_2 coatings. *ACS Applied Bio Materials* 2024; **7(8)**, 5579-5596.

[46] AM Mohammed, M Mohammed, JK Oleiwi, FH Ihmedee, T Adam, BO Betar and SCB Gopinath. Comprehensive review on zinc oxide nanoparticle production and the associated antibacterial mechanisms and therapeutic potential. *Nano Trends* 2025; **11**, 100145.

[47] W Elmer and JC White. The Future of nanotechnology in plant pathology. *Annual Review of Phytopathology* 2018; **56(1)**, 111-133.

[48] S Gaba, A Varma and A Goel. Protective and curative activity of biogenic copper oxide nanoparticles against Alternaria blight disease in oilseed crops: A review. *Journal of Plant Diseases and Protection* 2022; **129(2)**, 215-229.

[49] P Amornpitoksuk, S Suwanboon, S Sangkanu, A Sukhoom, N Muensit and J Baltrusaitis. Synthesis, characterization, photocatalytic and antibacterial activities of Ag-doped ZnO powders modified with a diblock copolymer. *Powder Technology* 2012; **219**, 158-164.

[50] RS Kumar, SHS Dananjaya, M De Zoysa and M Yang. Enhanced antifungal activity of Ni-doped ZnO nanostructures under dark conditions. *RSC Advances* 2016; **6(110)**, 108468-108476.

[51] K Hirota, M Sugimoto, M Kato, K Tsukagoshi, T Tanigawa and H Sugimoto. Preparation of zinc

oxide ceramics with a sustainable antibacterial activity under dark conditions. *Ceramics International* 2010; **36(2)**, 497-506.

[52] JD Torres, EA Faria, JR SouzaDe and AG Prado. Preparation of photoactive chitosan-niobium (V) oxide composites for dye degradation. *Journal of Photochemistry and Photobiology A: Chemistry* 2006; **182(2)**, 202-206.

[53] R Jiang, H Zhu, J Yao, Y Fu and Y Guan. Chitosan hydrogel films as a template for mild biosynthesis of CdS quantum dots with highly efficient photocatalytic activity. *Applied Surface Science* 2012; **258(8)**, 3513-3518.

[54] SHS Dananjaya, RS Kumar, M Yang, C Nikapitiya, J Lee and M De Zoysa. Synthesis, characterization of ZnO-chitosan nanocomposites and evaluation of its antifungal activity against pathogenic *Candida albicans*. *International Journal of Biological Macromolecules* 2018; **108**, 1281-1288.

[55] H Cui, Z Zhang, T Wang, J Hong, L Lei and S Wei. Uptake and translocation of ZnO nanoparticles in rice tissues studied by single particle-ICP-MS. *Atomic Spectroscopy* 2023; **44(5)**, 343-353.

[56] OA Capraru, B Lungu, M Virgolici, M Constantin, M Cutrubinis, L Chirila, LO Cinteza and I Stanculescu. Gamma irradiation and Ag and ZnO nanoparticles combined treatment of cotton textile materials. *Materials* 2022; **15(8)**, 2734.

[57] M Kaloti and A Kumar. Synthesis of chitosan-mediated silver coated γ-Fe_2O_3 (Ag–γ-Fe_2O_3@Cs) superparamagnetic binary nanohybrids for multifunctional applications. *Journal of Physical Chemistry C* 2016; **120**, 17627-17644.

[58] AA Wardana, P Kingwascharapong, LP Wigati, F Tanaka and F Tanaka. The antifungal effect against Penicillium italicum and characterization of fruit coating from chitosan/ZnO nanoparticle/Indonesian sandalwood essential oil composites. *Food Packaging and Shelf Life* 2022; **32**, 100849.

[59] AR Chowdhuri, S Tripathy, S Chandra, S Roy and SK Sahu. A ZnO decorated chitosan-graphene oxide nanocomposite shows significantly enhanced antimicrobial activity with ROS generation. *RSC Advances* 2015; **5(59)**, 49420-49428.

[60] K Hirota, M Sugimoto, M Kato, K Tsukagoshi, T Tanigawa and H Sugimoto. Preparation of zinc oxide ceramics with a sustainable antibacterial activity under dark conditions. *Ceramics International* 2010; **36(2)**, 497-506.

[61] HN Fones, DP Bebber, TM Chaloner, WT Kay, G Steinberg and SJ Gurr. Threats to global food security from emerging fungal and oomycete crop pathogens. *Nature Food* 2020; **1**, 332-342.